

Geochemistry, Monazite U–Pb Dating, and Li–Nd Isotopes of the Madi Rare Metal Granite in the Northeastern Part of the North China Craton



HOU Jianglong*, JIANG Biao and DAI Hongzhang

MNR Key Laboratory of Metallogeny and Mineral Assessment, Institute of Mineral Resources, Chinese Academy of Geological Sciences, Beijing 100037, China

Abstract: The Madi rare metal granite is a complex massif, which contains a variety of rare metals, such as Nb, Ta, Li, and Be. In this paper, the geochemical characteristics of the granite were obtained by multi-collector inductively coupled mass spectrometry (MC-ICP-MS). The precise crystalline age of the granite was obtained from monazite U–Pb dating, and the source of the granite was determined using Li–Nd isotopes. The Madi rare metal granite is a high-K (calc-alkaline), peraluminous, S-type granite. The U–Pb monazite age indicates that the crystalline age of the granite is 175.6 Ma, which is Early Jurassic. The granite is characterized by a relatively wide range of $\delta^7\text{Li}$ values (+2.99‰ to +5.83‰) and high lithium concentrations (181 ppm to 1022 ppm). The lithium isotopic composition of the granite does not significantly correlate with the degree of magmatic differentiation. An insignificant amount of lithium isotope fractionation occurred during the granitic differentiation. The lithium isotopic composition of the granite significantly differs from that of the wall rock, but it is very similar to that of a primitive mantle peridotite xenolith (mean $\delta^7\text{Li}$ value +3.5‰). The plot of Li concentration versus $\delta^7\text{Li}$ indicates that the Li isotopic composition of the granite is similar to that of island arc lavas. Based on the above-described evidence, the granite was mainly derived from the crust, but it was contaminated by a deep granitic magma.

Key words: geochemistry, U–Pb monazite age, Li–Nd isotopes, crystallization age, magmatic source, Madi rare metal granite

Citation: Hou et al., 2019. Geochemistry, Monazite U–Pb Dating, and Li–Nd Isotopes of the Madi Rare Metal Granite in the Northeastern Part of the North China Craton. *Acta Geologica Sinica (English Edition)*, 93(4): 901–911. DOI: 10.1111/1755-6724.13798

1 Introduction

Rare metal granites are an important source of rare metal resources and are widely distributed in the South China. However, they are rare in the North China Craton. The Madi granite is a complex massif that contains a variety of rare metal elements, such as Nb, Ta, Li, and Be.

Several previous studies determined crystallization age of this granite. Ye et al. (1987, 1991) reported a whole-rock Rb–Sr isochron age of 171 Ma, while Wang et al. (1994) reported an age of 166.3 Ma using the same analytical method. Because the Rb–Sr system is easily modified by ore-forming fluids, it is hard to determine the crystallization age of a granite using only Rb–Sr isochron age. Furthermore, the Madi granite is a highly differentiated granite, and the zircons in the granite have altered to cyrtolite. Thus, it is impossible to obtain an accurate U–Pb zircon age. Fortunately, the Madi granite contains monazite, which is suitable for constraining the crystalline age.

As to the source of the granite, Ye et al. (1987, 1991) suggested that the granite is the product of a deep magma which was subjected to full differentiation (Ye et al., 1987, 1991). It is well known that trace element modeling can reflect source characteristics, but it can not explain the

source of fluids. Similar geochemical characteristics can be explained using source characteristics and can be interpreted as fractional crystallization during metasomatism (Magna et al., 2008). Therefore, we need a more precise method to identify the source of the granite. The lithium isotopic system is an unconventional stable isotope system, which does not experience significant fractionation during high-temperature magmatic processes (Halama et al., 2007, 2008). Lithium isotopic fractionation mainly occurs during weathering (Rudnick et al., 2004; Kisakùrek et al., 2004). Therefore, lithium isotopes can serve as an effective constraint for determining the source of magmas.

In this paper, we investigated the geochemistry, crystalline age, and source of the Madi granite by geochemical analyses, monazite U–Pb dating, and Li–Nd isotopic analyses. Investigating the crystalline age and source of the Madi granite can improve research on rare metal deposits in the North China Craton and is also important for the evaluation of rare metal resources in the North China Craton.

2 Geologic Setting

The Madi granite is located in the southeastern part of Xinglong County at N40°17'1.18", E117°31'41.7" (Fig. 1). It is tectonically located in the western part of the Xinglong-Shanhaiguan uplift on the north margin of the

* Corresponding author. E-mail: houjianglong1988@126.com

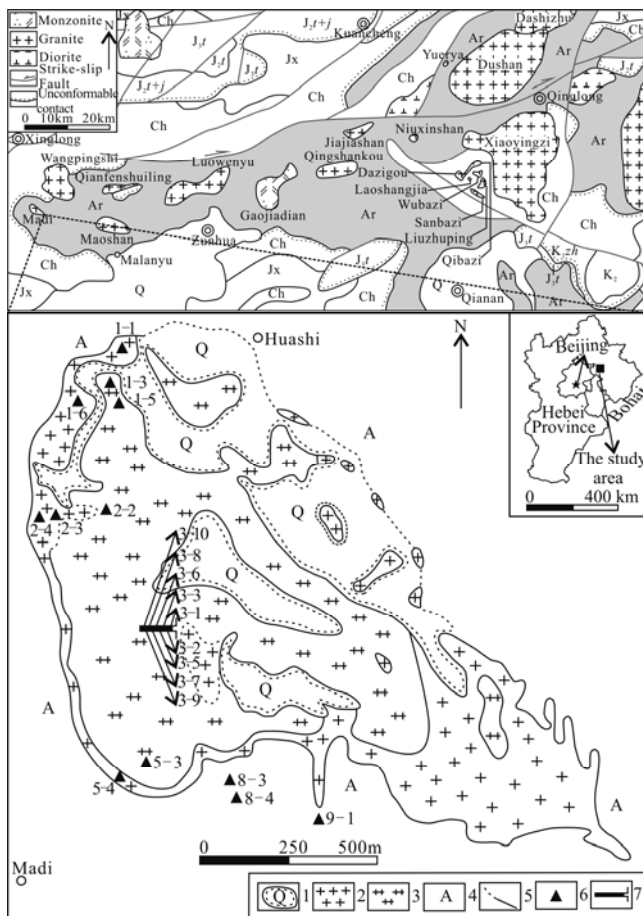


Fig. 1. Geological map of the Madi granite (after Yang et al., 2015; Ye et al., 2015).

Ar: Archean crystallized basement; Ch: Changcheng System; Jx: Jixian System; Qb: Qingbaikou System; J_1+J_2 : Jiulongshan-Tianjishan Formation; J_3 : Tuchengzi Formation; K_1zh : Zhangjiakou Formation; K_2 : Upper Cretaceous; Q: Quaternary; 1, Quaternary; 2, Zinnwaldite-albite granite; 3, Lepidolite-zinnwaldite-albite granite; 4, Archaean Sanggan Group gneiss; 5, Contact boundary attitude; 6, Location of samples; 7, Footrill.

North China Craton (NCC) (Ye et al., 2015; Li et al., 2017). It is part of the Malanyu-Suizhong Fe-Au-Pb-Zn secondary metallogenic belt (Xu et al., 2008). The wall rock of the granite is Paomachang Formation, which is mainly composed of plagioclase gneiss and magnetite quartzite. The Madi granite is located along the western axis of the Malanyu anticline, which is the main structure of the study area. The granite is gourd-shaped (Fig. 1; Regional Geology of Hebei Province, Beijing Municipality, and Tianjin Municipality Province, 1989) with the long axis striking NW310°. The granite is approximately 4200 m long and 800 m to 2010 m wide. The outcrop area of the granite is approximately 6 km².

The granite is a complex massif consisting of two stages: The first stage is a zinnwaldite-albite granite that mainly outcrops for about 1.2 km² in the southeast. The second stage is a lepidolite-zinnwaldite-albite granite that mainly outcrops for about 4.5 km² in the northwest. The zinnwaldite-albite granite is light red and has a fine-equigranular texture and a massive structure. It usually contains lath-shaped albite crystals a few millimeters in diameter. The lepidolite-zinnwaldite-albite granite is

offwhite has a unequigranular texture, and a massive structure. The granite in this stage exhibits a checkerboard texture and a snowball texture. Based on the structure of the granite, we conclude that the granite was emplaced from the southeast to the northwest.

3 Sampling and Analytical Methods

3.1 Sampling

The samples were collected from Madi village to Huashi village. We collected 21 whole-rock samples in this study.

3.2 Analytical methods

3.2.1 Major, trace, and rare earth element analyses

The major, trace, and rare earth element analyses were conducted at the National Research Center for Geoanalysis. The major element analyses were conducted using a PE8300 X-ray fluorescence spectrometer (XRF), and the trace element analyses were conducted using a PE300D inductively coupled mass spectrometer (ICP-MS). The samples analyzed for rare earth elements were dissolved with acid (HF+HNO₃) before ICP-MS analysis. In was used as the internal standard with a precision of 10⁻⁹. The quality of the analyses was determined using standards AMH-1 and OU-3 (international standard samples).

3.2.2 U-Pb monazite ages

The transmitted light, reflected light, and back scattered electron imaging (BSE) of the monazite crystals were all taken at the Nanjing Hongchuang Geological Prospecting Technology Limited Company. We used these monazite micrographs to choose appropriate areas for analysis, i.e., those areas without fractures, inclusions, or other impurities. The U-Pb monazite ages were obtained at the Tianjin Center, China Geological Survey using a laser ablation multi-collector inductively coupled plasma mass spectrometer (LA-MC-ICP-MS). The laser ablation system is a NEW WAVE 193 nm FX ArF excimer laser made by ESI. The wavelength of the laser was 193 nm, the pulse width was less than 4 ns, the diameter of the beam spot was 20 μm, the frequency of the pulse was 5 Hz, and the output power of laser was about 10–11 J/cm². The LA-MC-ICP-MS used is a NEPUNE made by Thermo Fisher. Its ion optical path has double the energy and quality focus. First, it uses dynamic zoom to expand the quality dispersion to 17%. The laser denudation material was sent to the MC-ICP-MS using He as the carrier gas (0.86 L/min) and Ar as the auxiliary gas (0.75 L/min). The U-Pb isotopes were simultaneously received by the zoom adjustment in order to enlarge the dispersion. Every sample required 20 s of gas background acquisition and 60 s of signal acquisition. Two monazite 44069 standards were analyzed between every 10 samples to correct for any U-Pb isotopic fractionation and instrument quality discrimination. We used the ²⁰⁷Pb correction method and isochron method for ordinary lead correction described by Andersen (2002). The data were processed using Isoplot, which was created by Ludwig (Ludwig, 2001). For detailed operating conditions and data processing

methods, see Cui et al. (2012).

3.2.3 Lithium isotopes

The chemical pretreatment and MC-ICP-MS analysis of the lithium isotopes were conducted at the MLR Key Laboratory of Metallogeny and Mineral Assessment. The chemical pretreatment process is as follows. First, 10 mg of the two-mica granite powder sample were weighed and placed in a PFA sample bottle with acid ($\text{HNO}_3:\text{HF}=1:5$). Then, the bottle was placed in an ultrasonicator for 10 min. The bottle was transferred to a hotplate and heated at 100–120°C for 24 h until it steamed and the grain size decreased. After this, concentrated HNO_3 was added to the bottle. Then, the bottle was transferred to a hotplate and heated at 100–120°C for 24 h, during which concentrated HNO_3 was added two to four times. Then, 3 ml of concentrated HCl was added, and the sample was heated for 24 h until it was dry. Finally, 4 mol/L HCl was added to the sample. Three cationic exchange resins (AG 50W-X8) were used to separate and purify the resulting solution. The $\delta^7\text{Li}$ analyses were conducted using a MC-ICP-MS. The $\delta^7\text{Li}$ values of international standards BHVO-2, AGV-2, and IRMM-016 were $+4.33\text{‰} \pm 0.76\text{‰}$ (2σ , $n=18$), $+5.68\text{‰} \pm 1.04\text{‰}$ (2σ , $n=18$), and $-0.01\text{‰} \pm 0.72\text{‰}$ (2σ , $n=15$), respectively (Tian et al., 2012). The analytical precision was similar to that of an international laboratory (Chan et al., 2002; Zack et al., 2003; Jeffcoate et al., 2004; Magna et al., 2004; Marschall et al., 2007; Qiu et al., 2009). The experimental procedure and mass spectrometry methods used are described by Su et al. (2011), Tian et al. (2012), and Zhao et al. (2015, 2017).

3.2.4 Nd Isotopes

The chemical pretreatment and MC-ICP-MS analyses of the Nd isotopes were both conducted at the National Research Center for Geoanalysis. The detailed chemical pretreatment process is as follows. First, 0.25 g of sample powder were weighed and placed in a TEFALON sample bottle with 0.5 ml of HNO_3 and 1.5 ml of HF in. The bottle was transferred to a hotplate, and heated at 190°C for 48 h. Then, ml of HNO_3 was added to the bottle, and the bottle was transferred to a hotplate and heated at 150°C for 6 h to achieve a constant solution volume of 25 g. Some of the sample solution was centrifuged, and the supernatant was collected. The supernatant was separated and purified using LN effect resin to obtain a solution with concentrated Nd. The $^{143}\text{Nd}/^{144}\text{Nd}$ analysis was conducted using a MC-ICP-MS. The quality fractionation correction for Nd was performed based on a $^{146}\text{Nd}/^{144}\text{Nd}$ value of 0.7218.

4 Results

4.1 Major, trace, and rare earth element analyses

The major, trace, and rare earth element compositions of the Madi granite are presented in Table 1.

4.2 U-Pb monazite ages

The U-Pb monazite ages of two samples (1–6 and 2–2) are presented in Table 2. Representative BSE images and U-Pb monazite ages of the Madi granite are shown in Fig. 2. The two monazite samples are light grey, with equiaxed

or short cylindrical euhedral crystals. The granularity of the monazite crystals varies from 50 μm to 200 μm . In the BSE images (Fig. 2), the monazite crystals have homogeneous structures and lack oscillatory zoning and corrosion rims. The U-Pb system of the monazite crystals is relatively simple. The weighted average age of the two intrusion stages are both 175.6 ± 1.1 Ma (Fig. 3), after removing outliers. The MSWD is approximately 0.70. This indicates that the U-Pb monazite age from the Madi granite is reliable and represents the crystallization age of the granite.

4.3 Li Isotopes

The lithium isotopic composition of the Madi granite is presented in Table 3. According to Table 3, the lithium concentrations of the wall rock vary from 10 ppm to 12 ppm with a mean value of 10.97 ppm. The $\delta^7\text{Li}$ values of the wall rock vary from -3.36‰ to -2.84‰ with a mean value of -3.04‰ . The lithium concentration of the contact zone between the granite and wall rock is 575 ppm, and its $\delta^7\text{Li}$ value is -1.32‰ . The lithium concentrations of the zinnwaldite-albite granite vary from 325 ppm to 993 ppm with a mean value of 540.40 ppm. The $\delta^7\text{Li}$ values of the zinnwaldite-albite granite vary from 2.99‰ to 5.78‰ with a mean value of 4.56‰ . The lithium concentrations of the lepidolite-zinnwaldite-albite granite vary from 181 ppm to 1022 ppm with a mean value of 357.20 ppm. The $\delta^7\text{Li}$ values of the lepidolite-zinnwaldite-albite granite vary from 4.00‰ to 5.83‰ with a mean value of 5.21‰ .

4.4 Nd Isotopes

The Nd isotopic composition of the Madi granite is presented in Table 4.

5 Discussion

5.1 Geochemical characteristics of the madi rare metal granite

The SiO_2 content of the Madi granite varies from 73.85% to 75.90% with a mean value of 75.21%. This indicates that the granite is silicic. The Na_2O contents of the two intrusions are both higher than their K_2O contents. The Na_2O content of the second intrusion is higher than that of the first intrusion; however, the K_2O content of the first intrusion is higher than that of the second. This

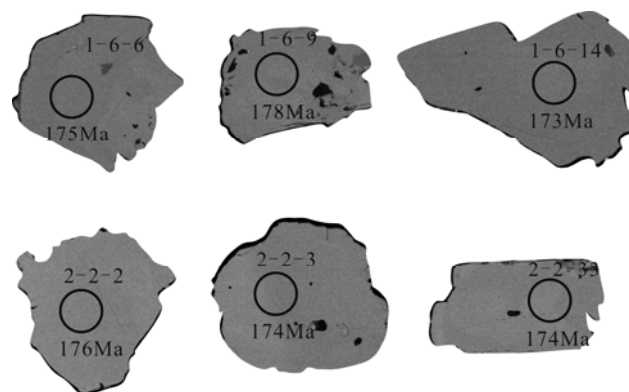


Fig. 2. Representative BSE images and U-Pb monazite ages of the Madi granite, Hebei province.

Table 1 Major, trace, and rare earth element compositions of the Madi granite

Samples	Zinnwaldite-albitegranite				Lepidolite-zinnwaldite-albitegranite					
	1-1	2-3	3-1	5-4	Average	1-3	2-2	3-2	5-3	Average
	Major elements (wt%)									
SiO ₂	75.81	74.89	75.90	75.49	75.52	75.52	74.43	75.77	73.85	74.89
Al ₂ O ₃	13.79	14.34	13.62	13.91	13.92	13.82	14.87	13.96	15.63	14.57
CaO	0.15	0.17	0.16	0.21	0.17	0.24	0.22	0.17	0.51	0.28
Fe ₂ O ₃	0.23	0.22	0.18	0.24	0.22	0.18	0.16	0.19	0.14	0.17
FeO	0.13	0.15	0.14	0.13	0.14	0.16	0.13	0.13	0.16	0.15
K ₂ O	4.02	4.08	4.31	4.05	4.12	4.03	3.89	4.05	2.15	3.53
MgO	0.08	0.08	0.09	0.08	0.08	0.07	0.08	0.08	0.12	0.09
MnO	0.18	0.17	0.25	0.24	0.21	0.20	0.16	0.21	0.05	0.15
Na ₂ O	4.91	5.08	4.64	4.95	4.90	4.95	5.24	4.96	6.79	5.48
P ₂ O ₅	0.01	0.01	0.01	0.01	0.01	0.01	0.01	0.01	0.01	0.01
TiO ₂	0.03	0.03	0.04	0.03	0.03	0.03	0.03	0.04	0.02	0.03
CO ₂	0.22	0.17	0.20	0.17	0.19	0.17	0.26	0.23	0.26	0.23
H ₂ O ⁺	0.27	0.30	0.31	0.25	0.28	0.21	0.26	0.32	0.36	0.29
Total	99.81	99.67	99.84	99.76	99.77	99.59	99.74	100.11	100.05	99.87
σ	2.43	2.63	2.44	2.49	2.50	2.48	2.65	2.48	2.59	2.55
A/CNK	1.52	1.54	1.50	1.51	1.52	1.50	1.59	1.52	1.65	1.57
A/NK	1.54	1.57	1.52	1.55	1.54	1.54	1.63	1.55	1.75	1.62
DI	97.29	97.00	97.16	96.92	97.09	96.97	96.42	97.10	95.48	96.49
AR	4.57	4.43	4.71	4.52	4.56	4.54	4.06	4.52	3.48	4.15
SI	0.80	0.83	0.91	0.85	0.85	0.75	0.84	0.88	1.28	0.94
FL	98.40	98.23	98.30	97.72	98.16	97.40	97.65	98.18	94.60	96.96
MF	82.56	81.82	78.75	82.22	81.34	82.93	78.38	79.51	71.43	78.06
OX	0.52	0.51	0.52	0.52	0.52	0.52	0.51	0.52	0.52	0.52
	Trace elements (ppm)									
Li	425.50	659.00	309.00	494.00	471.83	430.00	1022.00	294.00	9.90	438.89
Be	33.49	54.71	9.47	16.90	28.64	9.72	109.00	13.20	10.60	35.63
Cr	0.52	0.71	0.53	0.59	0.58	0.62	0.39	0.64	0.53	0.55
Mn	1167.00	1165.00	1876.00	1677.00	1471.08	1429.00	1119.00	1430.00	345.00	1080.83
Co	0.10	0.11	0.08	0.08	0.09	0.08	0.06	0.08	0.11	0.08
Ni	0.15	0.19	0.32	0.11	0.19	0.13	0.10	0.32	0.45	0.25
Cu	0.46	0.51	0.75	1.06	0.70	0.79	0.48	0.94	1.78	1.00
Zn	33.95	33.40	24.97	57.00	37.33	48.20	23.30	21.90	40.60	33.50
Ga	31.90	36.95	32.17	33.90	33.73	30.20	37.20	30.27	47.80	36.37
Rb	1524.00	1868.00	1214.00	1575.00	1545.13	1563.00	2287.00	1112.00	604.00	1391.50
Sr	1.05	2.07	8.90	4.28	4.07	1.70	3.21	6.90	21.80	8.40
Mo	0.16	0.25	0.47	1.46	0.58	0.26	0.06	0.48	0.27	0.27
Cd	0.02	0.04	0.16	0.23	0.11	0.04	0.02	0.09	0.41	0.17
In	0.21	0.20	0.12	0.21	0.18	0.19	0.15	0.12	0.09	0.14
Cs	42.90	162.10	48.60	48.50	75.53	43.20	303.00	61.50	4.56	103.07
Ba	1.84	4.18	24.25	3.93	8.55	2.07	1.32	29.50	53.00	21.47
Tl	8.03	9.01	6.15	7.79	7.74	7.97	11.00	5.47	2.72	6.79
Pb	22.00	30.50	26.28	33.00	27.95	38.90	29.60	29.13	12.60	27.56
Bi	6.68	3.87	1.88	13.50	6.48	5.90	7.96	0.99	1.58	4.11
Th	9.16	10.80	9.51	11.20	10.17	10.20	10.40	11.30	8.26	10.04
U	13.95	14.71	5.52	16.50	12.67	17.00	18.50	4.27	4.79	11.14
Nb	128.00	118.00	123.00	119.00	121.79	117.00	90.00	124.00	46.00	94.15
Ta	27.60	36.60	30.90	28.80	30.96	26.10	38.00	25.30	48.90	34.57
Zr	55.85	48.05	50.90	53.10	51.98	53.50	39.40	50.87	22.30	41.52
Hf	7.99	7.92	7.03	7.95	7.72	7.82	8.11	7.44	7.33	7.68
Sn	16.60	19.10	13.10	16.90	16.43	16.40	20.80	12.47	9.68	14.84
Sb	0.09	1.04	0.32	0.13	0.39	0.05	2.10	0.27	0.09	0.63
Ti	181.50	176.50	204.33	186.00	187.08	179.00	168.00	192.67	100.00	159.92
W	0.58	0.72	1.48	0.85	0.91	0.62	0.58	1.97	1.78	1.24
As	0.13	2.86	3.38	0.36	1.68	0.24	1.51	4.01	0.64	1.60
V	0.59	0.59	1.04	1.07	0.82	0.45	0.43	1.09	0.56	0.63
Sc	6.86	11.57	7.45	7.69	8.39	4.67	9.80	5.82	3.05	5.83
Y	6.64	9.04	11.32	14.10	10.27	7.20	5.56	7.22	1.27	5.31
	Rare earth elements (ppm)									
La	5.69	6.61	7.04	7.66	6.75	5.27	5.01	6.12	6.62	5.76
Ce	11.00	15.25	12.43	17.60	14.07	16.50	15.60	15.53	18.90	16.63
Pr	2.48	3.14	3.05	3.30	2.99	2.39	2.60	2.61	2.68	2.57
Nd	8.28	11.00	11.10	12.20	10.65	8.28	8.94	9.35	7.14	8.43
Sm	2.31	3.64	3.48	4.86	3.57	2.46	3.25	2.94	2.46	2.78
Eu	0.01	0.02	0.03	0.02	0.03	0.01	0.01	0.03	0.03	0.03
Gd	1.72	2.68	2.72	4.23	2.83	1.99	2.38	2.12	1.30	1.95
Tb	0.23	0.34	0.36	0.54	0.37	0.26	0.25	0.27	0.15	0.23
Dy	0.94	1.19	1.50	1.98	1.40	1.00	0.76	1.01	0.40	0.79
Ho	0.11	0.11	0.16	0.20	0.14	0.10	0.06	0.11	0.03	0.09
Er	0.20	0.20	0.30	0.34	0.26	0.20	0.08	0.20	0.03	0.16
Tm	0.03	0.03	0.04	0.04	0.03	0.02	0.01	0.03	0.01	0.03

Continued Table 1

Samples	Zinnwaldite-albitegranite					Lepidolite-zinnwaldite-albitegranite				
	1-1	2-3	3-1	5-4	Average	1-3	2-2	3-2	5-3	Average
Yb	0.17	0.16	0.26	0.29	0.22	0.17	0.09	0.17	0.03	0.14
Lu	0.02	0.02	0.03	0.03	0.03	0.02	0.01	0.02	0.01	0.02
REE	33.11	44.36	42.49	53.20	43.29	38.62	39.02	40.50	39.65	39.45
LREE	29.77	39.65	37.13	45.64	38.05	34.91	35.41	36.58	37.83	36.18
HREE	3.40	4.72	5.36	7.65	5.28	3.76	3.64	3.92	1.96	3.32
L/H	8.75	8.41	6.93	5.97	7.52	9.28	9.73	9.34	19.30	11.91
δEu	0.01	0.02	0.03	0.01	0.02	0.01	0.01	0.03	0.05	0.03
δCe	0.70	0.80	0.65	0.84	0.75	1.12	1.03	0.94	1.08	1.04

Table 2 U-Pb monazite ages for the Madi granite, Hebei Province

Samples	Isotope ratio						Age(Ma)					
	$^{207}\text{Pb}/^{206}\text{Pb}$	1σ	$^{207}\text{Pb}/^{235}\text{U}$	1σ	$^{206}\text{Pb}/^{238}\text{U}$	1σ	$^{207}\text{Pb}/^{206}\text{Pb}$	1σ	$^{207}\text{Pb}/^{235}\text{U}$	1σ	$^{206}\text{Pb}/^{238}\text{U}$	1σ
1-6-3	0.0498	2.4295	0.1907	2.5352	0.0277	0.9641	187	5	177	4	176	2
1-6-6	0.0503	2.8977	0.1907	2.9983	0.0275	1.0079	206	6	177	5	175	2
1-6-9	0.0499	2.1186	0.1923	2.2039	0.0280	0.9598	191	4	179	4	178	2
1-6-14	0.0501	2.5915	0.1882	2.7976	0.0272	0.9640	198	5	175	5	173	2
1-6-16	0.0495	2.0647	0.1870	2.1179	0.0274	0.9614	172	4	174	4	174	2
1-6-24	0.0505	1.5014	0.1927	1.6734	0.0277	0.9823	217	3	179	3	176	2
1-6-27	0.0496	2.0571	0.1884	2.1588	0.0275	0.9650	176	4	175	4	175	2
1-6-31	0.0498	1.8858	0.1896	1.9754	0.0276	0.9610	187	4	176	3	176	2
1-6-34	0.0498	2.1409	0.1916	2.3897	0.0279	0.9706	187	53	178	51	177	2
1-6-39	0.0500	1.9726	0.1905	2.0691	0.0277	0.9634	195	4	177	4	176	2
1-6-40	0.0508	1.8689	0.1937	1.9824	0.0277	0.9643	232	4	180	4	176	2
2-2-2	0.0504	2.1894	0.1923	2.2963	0.0276	0.9667	217	5	179	4	176	2
2-2-3	0.0501	3.2003	0.1899	3.3299	0.0274	0.9787	198	6	177	6	174	2
2-2-21	0.0495	9.3876	0.1891	9.8319	0.0276	1.1184	172	16	176	17	176	2
2-2-22	0.0502	2.0270	0.1939	2.1745	0.0280	0.9748	211	4	180	4	178	2
2-2-24	0.0502	3.6020	0.1930	4.2796	0.0276	1.2039	211	8	179	8	176	2
2-2-26	0.0496	3.7141	0.1909	3.8284	0.0279	0.9880	189	7	177	7	177	2
2-2-30	0.0511	4.7044	0.1965	4.7628	0.0279	1.0261	243	11	182	9	177	2
2-2-31	0.0506	2.5535	0.1911	2.6257	0.0274	0.9503	220	6	178	5	174	2
2-2-33	0.0501	1.5190	0.1893	1.6650	0.0274	0.9546	211	3	176	3	174	2
2-2-35	0.0500	2.4070	0.1885	2.5402	0.0273	0.9654	195	5	175	4	174	2

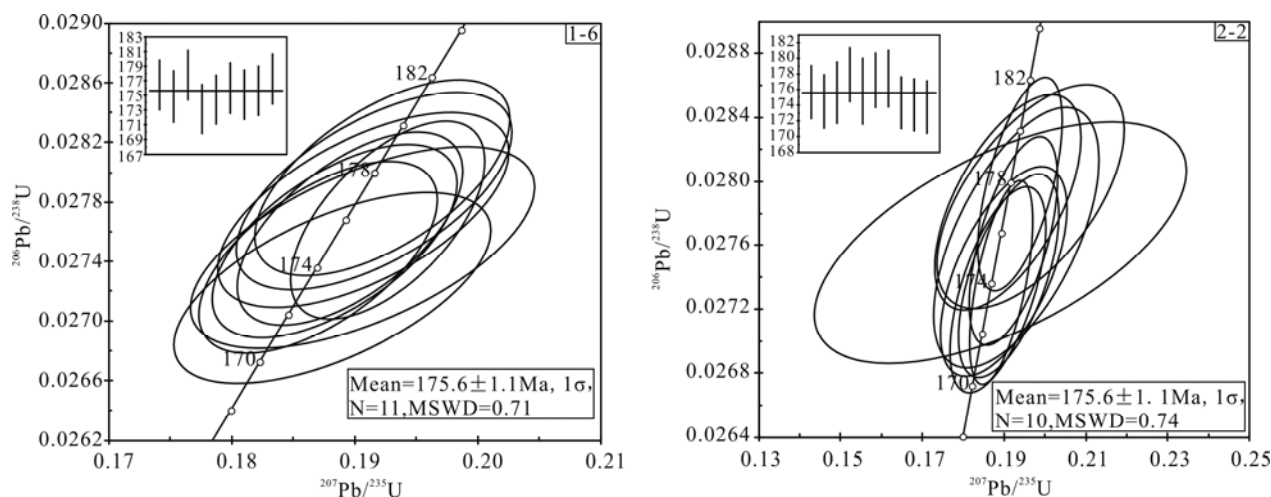


Fig. 3. LA-ICP-MS U-Pb concordia diagrams of monazites from the Madi granite.

indicates that the Madi granite gradually evolved from high potassium and low sodium to low potassium and high sodium as emplacement continued. The mean Rittmann Indexes (σ) of the two intrusions are both less than one, which indicates that the Madi granite is a calc-alkaline granite. The SiO_2 vs K_2O plot also indicates that the Madi granite is a high-K (calc-alkaline) granite (Fig. 4a). The A/CNK values of the two intrusions vary from 1.52 to 1.65 with a mean value of 1.54, which indicates that the granite is a peraluminous S-type granite (Fig. 4b). The

differentiation index (DI) of the Madi granite varies from 95.48 to 97.29. The solidification index (SI) varies from 0.75 to 1.28. This indicates that the degree of magmatic differentiation of the Madi granite is high. The felsic index (FL) of the Madi granite varies from 94.60 to 98.40. The ferromagnesian index (MF) of the Madi granite varies from 71.43 to 82.93, and the oxidation rate (OX) of the Madi granite varies from 0.51 to 0.52. This indicates that the degree of fractional crystallization was high.

The primitive mantle normalized spider diagram (Fig.

Table 3 Li isotopic composition of the Madi granite, Hebei province

Samples	$\delta^7\text{Li} \pm 2\sigma$ (‰)
ArchaeanSanggan Group gneiss	
8-3	-2.93±0.07
8-4	-2.84±0.04
9-1	-3.36±0.07
the contact plane of the granite and wall rock	
3-1	-1.32±0.02
Zinnwaldite-albite-granite	
1-1	4.93±0.02
2-3	5.78±0.03
2-4	4.22±0.02
3-8	2.99±0.03
5-4	4.88±0.02
Lepidolite-zinnwaldite-albite-granite	
1-3	4.91±0.02
1-5	5.12±0.02
2-2	5.83±0.03
3-2	5.52±0.03
3-3	5.33±0.02
3-5	5.28±0.02
3-6	5.73±0.02
3-7	5.29±0.02
3-9	5.13±0.02
3-10	4.00±0.02

5) of the Madi granite shows that the trace elements of the Madi granite have multiple enrichments and depletions. It is enriched with Rb, U, Ta, Nd, Hf, and Tb, and it is depleted in Ba, Sr, P, Eu, and Ti. It is significantly enriched with large ion lithophile elements (LILE) such as Rb, significantly depleted in Ba and Sr and high field strength elements (HFSE), such as Ti.

The REE pattern of the Madi granite (Fig. 6) shows that the granite has low rare earth element content (33.11 ppm to 53.20 ppm). There is significant fractionation between the light and heavy rare earth elements (LREE/HREE varies from 5.97 to 19.3). The LREE are significantly enriched, while the HREE are relatively depleted. The δEu

value varies from 0.01 to 0.05 with a mean value of 0.02, which indicates that the Madi granite is extremely depleted in Eu. The δCe value varies from 0.65 to 1.12 with a mean value of 0.90, which indicates that the Madi granite is also depleted in Ce. The REE pattern of the Madi granite shows that the trends of all of the elements are basically the same, indicating that the Madi granite is the product of homologous magma evolution or that it is from the same source region.

5.2 Crystallization age of the madi granite and its geological significance

The weighted average age of the two intrusions is 175.6 Ma (Figs. 2 and 3). This age is relatively close to the 171 Ma whole-rock Rb-Sr isochron age obtained by Ye et al. (1987). The age of the monazite provides another accurate constraint on the crystallization age of the granite, which indicates that the granite was emplaced in the Early Jurassic. The ages of two intrusions are nearly identical, which suggests that the two intrusions are the product of a cognate magma.

In this study, we determined the U-Pb monazite age of the Madi granite. The chronological study of the Mesozoic acid intrusive granites by Yang et al. (2015) concluded that the formation ages ranged from the Late Permian to the Late Jurassic. There are two peak ages in the Late Triassic (224–186 Ma) and in the Early Jurassic (180–153 Ma). The main formation occurred in the Early Jurassic. The Madi granite is a rare metal granite formed in the Early Jurassic. The Madi granite formed later in the Malanyu anticlinorium. This suggests that other intrusions with the same or similar formation ages, located in the Malanyu compound anticline, may also have rare metal mineralization. However, further research is required to verify this hypothesis. Based on the above discussion, U-Pb monazite age of the Madi complex massif provides

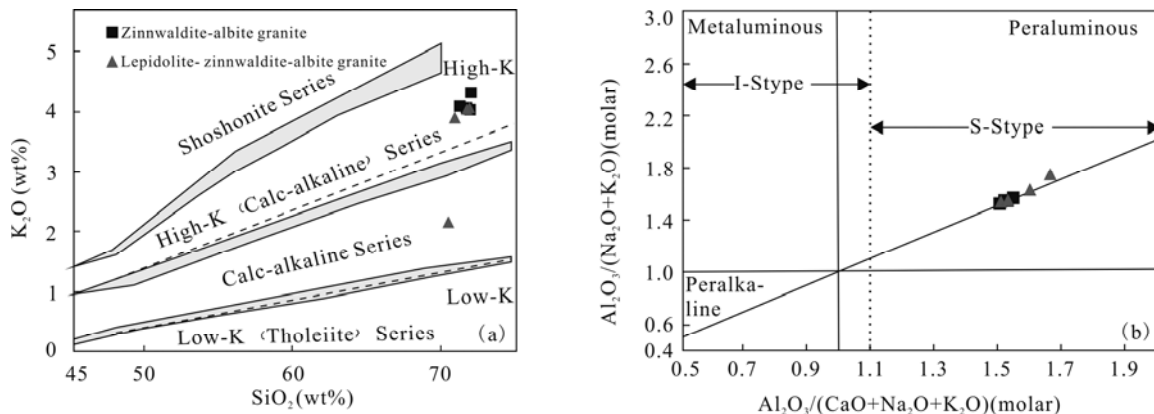


Fig. 4. Plots of SiO_2 vs K_2O (Rickwood, 1989) and A/CNK vs A/NK (Maniar et al., 1989) (a. SiO_2 vs K_2O diagram; b. A/CNK vs A/NK).

Table 4 Nd isotopic composition of the Madi granite

Sample	Sm(ppm)	Nd(ppm)	$^{147}\text{Sm}/^{144}\text{Nd}$	$^{143}\text{Nd}/^{144}\text{Nd}$	$(^{143}\text{Nd}/^{144}\text{Nd})_t$ ($t=175.6\text{Ma}$)	$\epsilon_{\text{Nd}}(t)$
1-1	0.39	1.47	0.15948	0.51187	0.51168	-14.21
1-3	0.69	2.44	0.17068	0.51190	0.51170	-13.85
2-2	1.13	3.77	0.18051	0.51190	0.51169	-14.12
3-1	0.49	1.53	0.19271	0.51189	0.51167	-14.53
3-2	1.57	4.39	0.21669	0.51190	0.51165	-14.92
5-3	0.46	1.79	0.15706	0.51186	0.51168	-14.30
5-4	0.38	1.17	0.19675	0.51191	0.51169	-14.15

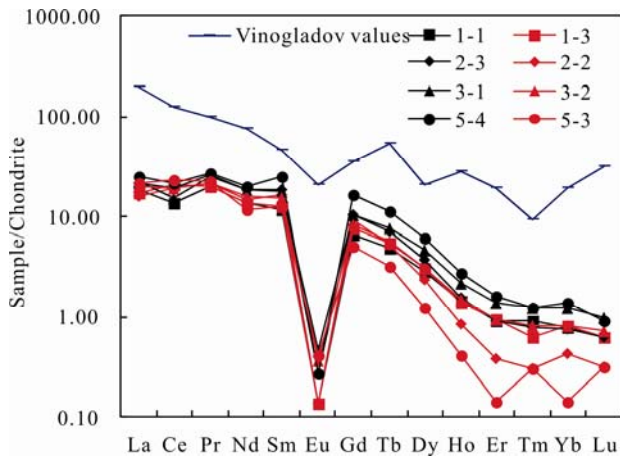


Fig. 5. Primitive mantle-normalized trace element patterns for the Madi granite.

new data to constrain the crystallization age of the Madi granite, the formation of the Malanyu compound anticline, and the tectonic evolution of Yanshan in the Mesozoic. This has important practical significance.

5.3 Lithium Isotopic Composition and Fractionation of the Madi Granite

According to Table 3, the Madi granite has a relatively high Li concentration (mean 418.27 ppm) and high $\delta^7\text{Li}$ values (mean +5.00‰) compared to the world granite (mean Li concentration 66.8 ppm, mean $\delta^7\text{Li}$ value +1.4‰; Bryant et al., 2004; Teng et al., 2004, 2006, 2009;

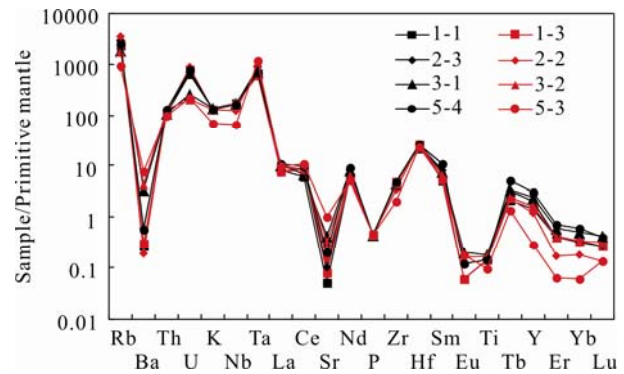


Fig. 6. Chondrite-normalized REE patterns for the Madi granite.

Magna et al., 2010; Romer et al., 2014; Wang et al., 2017). As per statistics, the $\delta^7\text{Li}$ values of the granites vary from -10‰ to +20‰ (Tomascak, 2004). The $\delta^7\text{Li}$ values of I-stype granites vary from -2.5‰ to +8.0‰, the $\delta^7\text{Li}$ values of A-stype granites vary from -1.8‰ to +6.9‰, and the $\delta^7\text{Li}$ values of S-stype granites vary from -1.56‰ to +9‰. The Madi granite is an S-stype granite. It has significantly different $\delta^7\text{Li}$ values than those of the New England S-type granite in eastern Australia, but it has similar $\delta^7\text{Li}$ values to the Jingshan leucogranite in Anhui Province (Fig. 4) (Bryant et al., 2004; Teng et al., 2004, 2006, 2008, 2009; Tomascak, 2004; Su et al., 2010; Sun et al., 2016). In terms of its lithium isotopic composition, the Madi granite is significantly enriched in ^7Li (Fig. 7).

Lithium isotopic fractionation is related to many factors,

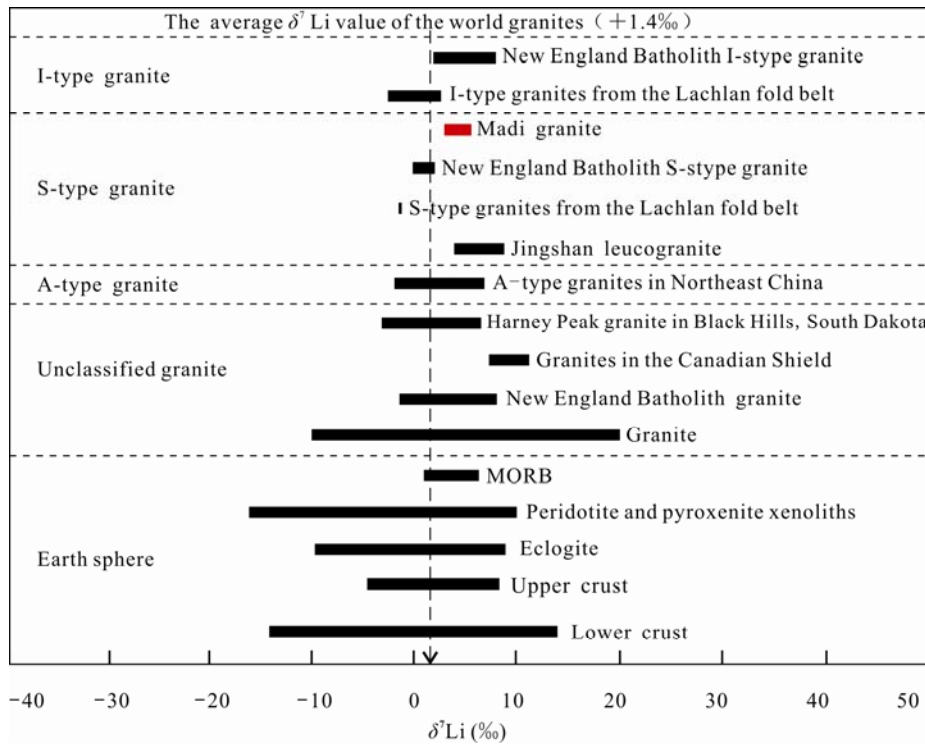


Fig. 7. Lithium isotopic composition of various granites.

Note: data for the unclassified granite from Su et al., 2010; data for the Jingshan leucogranite from Sun et al., 2016; data for the S-type and I-type granites from the Lachlan fold belt from Teng et al., 2004; data for the lower crust from Teng et al., 2008; data for the A-type granites from Northeastern China from Teng et al., 2009; data for the New England S-type Batholith and I-type granites from Bryant et al., 2003; data for the granites from the Canadian Shield from Tomascak et al., 2004; data for the Harney Peak granite from the Black Hills, South Dakota from Teng et al., 2006)

such as temperature and diffusion; however, there is no consensus of the mechanism of lithium isotopic fractionation (Tang et al., 2009; Richter et al., 2009, 2014). There is negligible ($\leq 1.0\%$) lithium isotopic fractionation during the high temperature process of magmatic ascent (Halama et al., 2007, 2008) and the anatexis of the crust (Bryant et al., 2004; Teng et al., 2004). However, lithium isotopic fractionation occurs during weathering (Rudnick et al., 2004), interaction between the magma and wall rock, and the fractional crystallization of granites and pegmatite formation at 340°C – 600°C (Teng et al., 2006).

Fractional crystallization of granite is one of the most important factors that affect lithium isotopic fractionation. During crystallization, quartz preferentially takes ^7Li into its two- and four-fold-coordinate interstitial sites. thus, positive correlations between $\delta^7\text{Li}$ and Li and between $\delta^7\text{Li}$ and SiO_2 should be observed (Halama et al., 2007). However, there is no correlation between $\delta^7\text{Li}$ and Li or between $\delta^7\text{Li}$ and SiO_2 in the Madi granite (Fig. 8). In addition, the $\delta^7\text{Li}$ and $\varepsilon_{\text{Nd}}(t)$ values of the Madi granite are not correlated (Fig. 8). This indicates that equilibrium lithium isotopic fractionation occurred during the fractional crystallization of the Madi granite.

5.4 Tectonic Setting and Material Source of the Madi granite

It is believed that most peraluminous S-type granites

were formed during the contraction and stacking stage of the Earth's crust during syn-collisional periods. S-type granites are mainly formed by remelting of the middle or upper crust (Pitcher, 1983; Pearce et al., 1984; Harris et al., 1986). On the plot of $\text{Yb}+\text{Ta}$ vs Rb (Pearce et al., 1984) (Fig. 9a) and the $\text{Rb}/30\text{-Hf-Ta}\times 3$ diagram (Harris et al., 1986) (Fig. 9b), the majority of the samples fall within the syn-collision field and only one sample fall within the within plate granites (WPG) field. This indicates that the Madi granite was formed during the late stage of a syn-collisional period, i.e., the stage when collision transitions to extension. This further indicates that the Malanyu uplift formed in a collisional environment during thickening of the Earth's crust in the Mesozoic.

The sources of peraluminous granites are mainly clastic sedimentary rocks and metamorphic sedimentary rocks in the crust (Sylvester, 1998). Based on experimental petrology, Douce (1998) concluded that peraluminous granites are only formed by partial melting of muddy and sandy sedimentary rocks. On the $\text{Al}_2\text{O}_3/\text{TiO}_2$ versus $\text{CaO}/\text{Na}_2\text{O}$ plot, the samples are all located near the Shisga Pangma of Himalayan orogenic belt (Fig. 10a) (Sylvester, 1989). On the Rb/Sr vs Rb/Ba plot, all of the samples plot within the rich clay field (Fig. 10b; Sylvester, 1989). This indicates that the source of the Madi granite is mainly mudstone. The $t\text{-}\varepsilon_{\text{Nd}}(t)$ diagram provides more proof that the material source of the granite maybe was the continental crust (Fig. 11).

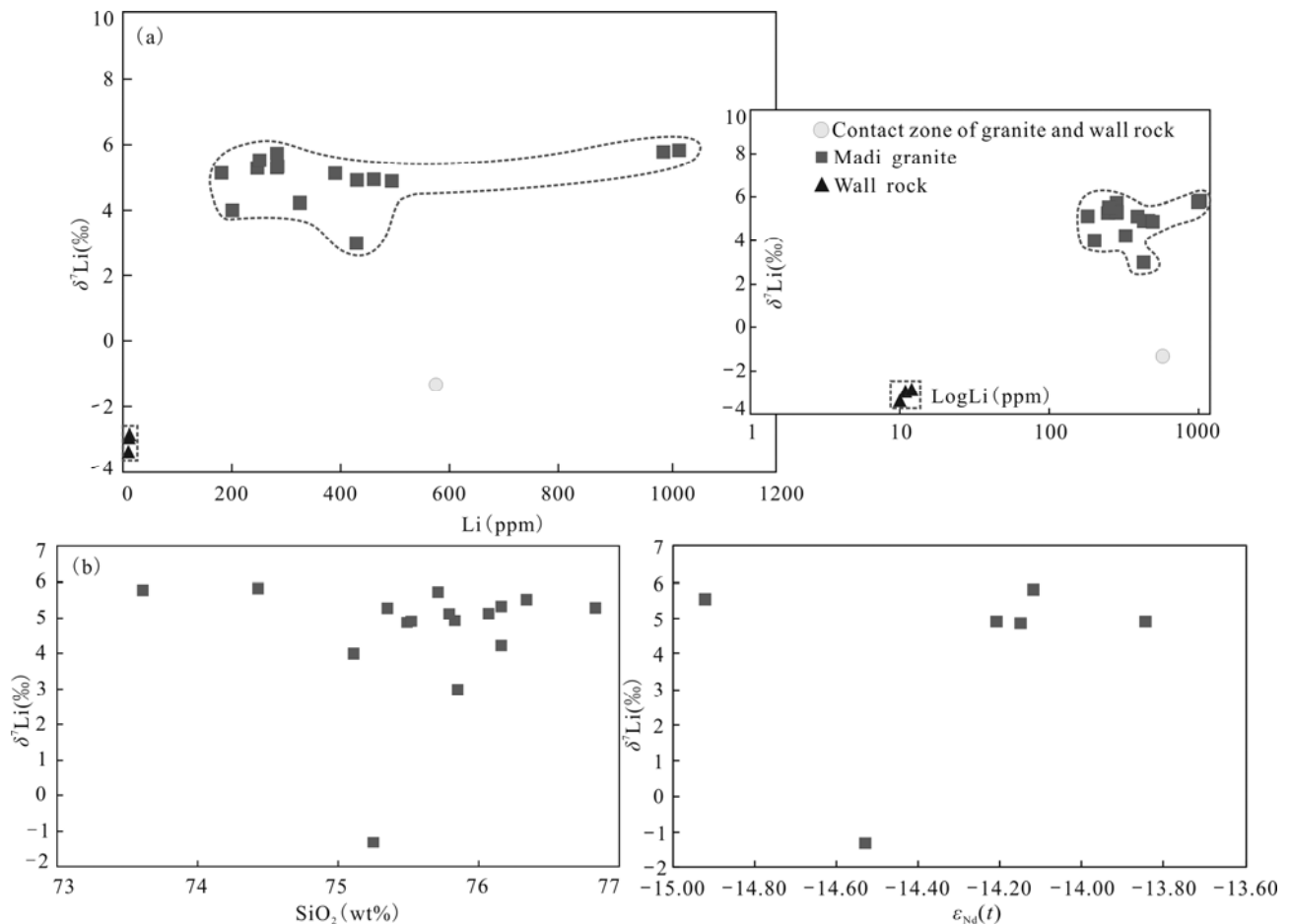


Fig. 8. Plots of $\delta^7\text{Li}$ vs Li, and SiO_2 vs $\varepsilon_{\text{Nd}}(t)$ for the Madi granite

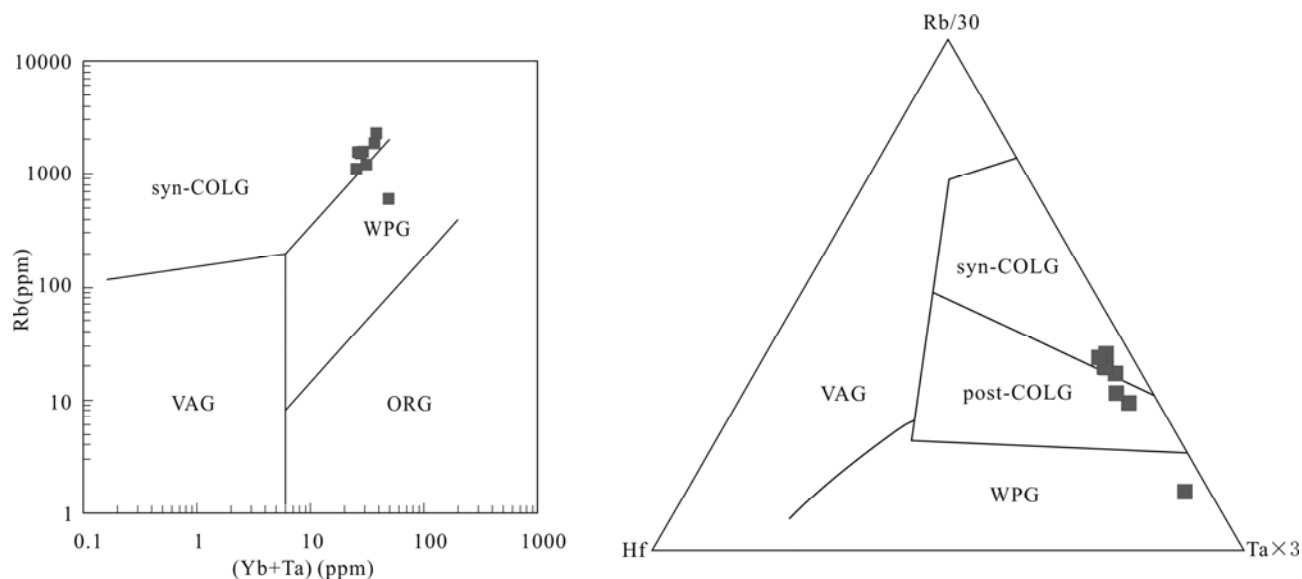


Fig. 9. Plots of Yb+Ta vs Rb (Pearce et al., 1984) and Rb/30 vs Hf-Ta \times 3 (Harris et al., 1986) for the Madi granite.

ORG: ocean ridge granites; VAG: volcanic arc granites; WPG: within plate granites; syn-COLG: syn-collisional granites; post-COLG: post-collisional granites

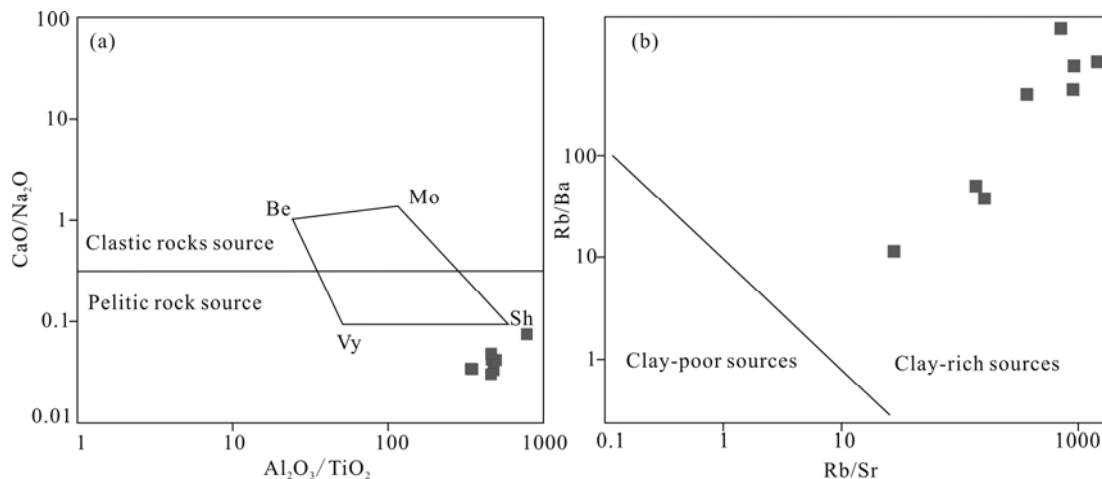


Fig. 10. Plots of CaO/Na₂O vs Al₂O₃/TiO₂ and Rb/Ba vs Rb/Sr for the Madi granite (after Sylvester, 1989).

Be: Bethanga; Mo: Moschumandl; Vy: Vysoky Kamen; Sh: Shisga Pangma

According to Table 3, the mean $\delta^7\text{Li}$ values of the granite and wall rock are -3.04‰ to -1.32‰ and 4.56‰ to 5.21‰ , respectively. The mean $\delta^7\text{Li}$ value gradually increases. The $\delta^7\text{Li}$ values of the wall rock are negative and remain stable, varying by only 0.52‰ . However, the $\delta^7\text{Li}$ values of the granite are positive and vary significantly, varying by 2.84‰ . The $\delta^7\text{Li}$ values of the granite and the wall rock differ by more than 5.83‰ . This indicates that there is a significant difference between the lithium isotopic composition of the granite and the wall rock. The mean $\delta^7\text{Li}$ value of the Madi granite ($+5\text{‰}$) is higher than that of the Earth's crust ($0\pm 2\text{‰}$) (Teng et al., 2004), but it is very close to that of primitive mantle peridotite xenoliths (mean $\delta^7\text{Li}$ value $+3.5\text{‰}$) (Tomascak et al., 2008). This suggests that the source of the Madi granite was contaminated with deep granitic magma. Plots of Li concentration versus $\delta^7\text{Li}$ (Fig. 6; Tang et al., 2007, 2011) shows that the Li isotopic composition of the Madi granite is similar to that island arc lavas (-6‰ to $+12\text{‰}$;

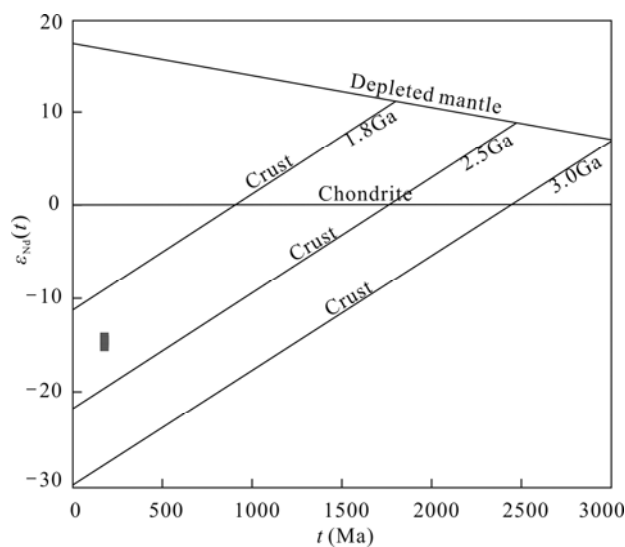


Fig. 11. t - $\epsilon_{\text{Nd}}(t)$ diagram of the Madi granite

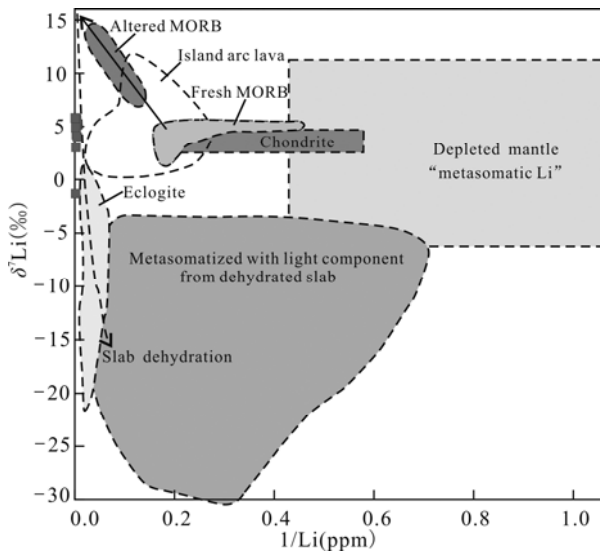


Fig. 12. Plot of Li concentrations versus $\delta^7\text{Li}$ (Tang et al., 2011)

primarily from +2‰ to +6‰). The above facts suggest that the main material source of the Madi granite is crustal material contaminated by deep granitic magma (Fig. 12).

6 Conclusions

(1) The Madi rare metal granite is a high-K (calc-alkaline), peraluminous, S-type granite. The two intrusions of the Madi granite are likely the product of the homologous magmatic evolution or of the same source region.

(2) The U-Pb monazite age indicates that the crystalline age of the Madi rare metal granite is 175.6 Ma (the Early Jurassic).

(3) The lithium concentrations of the Madi granite vary from 181 ppm to 1022 ppm, and the $\delta^7\text{Li}$ values of the granite vary from +2.99‰ to +5.83‰. The granite has high lithium concentration and high $\delta^7\text{Li}$ values. Equilibrium lithium isotopic fractionation occurring during the fractional crystallization of the Madi granite seems unlikely. The lithium isotopic composition of the Madi granite was likely inherited from the source rocks, which is not affected by differentiation and alteration of the magma.

(4) The Madi granite was formed during the late stage of a syn-collision period. Analysis of the lithium isotopes and Nd isotopes indicate that the main source of the Madi granite is crust contaminated by deep granitic magma.

Acknowledgments

This work is granted by the project of "Comprehensive integration and service of mineral geology and its metallogenic regularity in China" from China Geological Survey (Grant No.DD20160346).

Manuscript received Jan. 13, 2018
 accepted Oct. 12, 2018
 associate EIC MAO Jingwen
 edited by FEI Hongcai

References

- Andersen, T., 2002. Correction of common lead in U-Pb analyses that do not report ^{204}Pb . *Chemical Geology*, 192(1–2): 59–79.
- Bryant, C.J., Chappell, B.W., Bennett, V.C., and McCulloch, M.T., 2004. Lithium isotopic compositions of the New England Batholith: correlations with inferred source rock compositions. *Transactions of the Royal Society of Edinburgh: Earth Sciences*, 95: 199–214.
- Chan, L.H., Starinsky, A., and Katz, A., 2002. The behavior of lithium and its isotopes in oilfield brines: evidence from the Heletz-Kokhav field, Israel. *Geochimica et Cosmochimica Acta*, 66: 615–623.
- Cui, Y.R., Zhou, H.Y., Geng, J.Z., Li, H.K., and Li, H.M., 2012. In situ LA-MC-ICP-MS U-Pb isotopic dating of Monazite. *Acta Geoscientica Sinica*, 33(6): 865–876 (in Chinese with English abstract).
- Halama, R., McDonough, W.F., Rudnick, R.L., Keller, J., and Klaudius, J., 2007. The Li isotopic composition of Oldoinyo Lengai: nature of the mantle sources and lack of isotopic fractionation during carbonatite petrogenesis. *Earth and Planetary Science Letters*, 254: 77–89.
- Halama, R., McDonough, W.F., Rudnick, R.L., and Bell, K., 2008. Tracking the lithium isotopic evolution of the mantle using granitic carbonatites. *Earth and Planetary Science Letters*, 265: 726–742.
- Harris, N.B.W., Pearce, J.A., and Tindle, A.G., 1986. *Geochemical characteristics of collision-zone magmatism*. Geological Society London, Special Publications, 19: 67–81.
- Hebei Bureau of Geology and Minerals., 1989. *Regional geology of Hebei Province*, Beijing Municipality, and Tianjin Municipality. Beijing: Geological Publishing House, 748 (in Chinese).
- Jeffcoate, A.B., Elliott, T., Thomas, A., and Bouman, C., 2004. Precise, small sample size determinations of lithium isotopic compositions of geological reference materials and modern seawater by MC-ICPMS. *Geostandards and Geoanalytical Research*, 28: 161–172.
- Kisakürek, B., Widdowson, M., and James, R.H., 2004. Behavior of Li isotopes during continental weathering: the Bidar laterite profile, India. *Chemical Geology*, 212: 27–44.
- Li, Y.J., Xie, W., Qi, Y.F., Miao, Q.F., Xiong, C., and Gong, C.W., 2017. A super-large Rb-Nb rare metal deposit has been discovered in Huashi village of Xinglong county, Hebei Province. *Acta Geologica Sinica (English Edition)*, 91(6): 2344–2345.
- Ludwig, K.R., 2001. *User's manual for Isoplot/Ex (rev.2.49): a geochronological toolkit for Microsoft Excel*. Berkeley: Geochronology Center Special Publication: 1–55.
- Magna, T., Wiechert, U.H., and Halliday, A.N., 2004. Low-blank isotope ratio measurement of small samples of lithium using multiple-collector ICPMS. *International Journal of Mass Spectrometry and Ion Processes*, 239: 67–76.
- Magna, T., Ionov, D.A., Oberli, F., and Wiechert, U., 2008. Links between mantle metasomatism and lithium isotopes: evidence from glass-bearing and cryptically metasomatized xenoliths from Mongolia. *Earth and Planetary Science Letters*, 276: 214–222.
- Magna, T., Janoušek, V., Kohút, M., Oberli, F., and Wiechert, U., 2010. Finger printing sources of orogenic plutonic rocks from variscan belt with lithium isotopes and possible link to subduction-related origin of some A-type granites. *Chemical Geology*, 274: 94–107.
- Maniar, P.D., and Piccoli, P.M., 1989. Tectonic discrimination of granitoids. *Geological Society of America Bulletin*, 101: 635–643.
- Marschall, H.R., Pogg von Strandmann, P.A.E., Seitz, H.M., Elliott, T., and Niu Yaoling., 2007. The lithium isotopic composition of orogenic eclogites and deep subducted slabs. *Earth and Planetary Science Letters*, 262: 563–580.
- Patiño Douce, A.E., and Harris, N., 1998. Experimental constraints on Himalayan anatexis. *Journal of Petrology*, 39(4): 689–710.
- Pearce, J.A., Harris, N.B.W., and Tindle, A.G., 1984. Trace element discrimination diagrams for the tectonic interpretation of granitic rocks. *Journal of Petrology*, 25(4): 956–983.

- Qiu, L., Rudnick, R.L., McDonough, W.F., and Merriman, R.J., 2009. Li and $\delta^7\text{Li}$ in mudrocks from the British Caledonides: metamorphism and source influences. *Geochimica et Cosmochimica Acta*, 73: 7325–7340.
- Pitcher, W.S., 1983. Granite type and tectonic environment. In: Hsu K ed. *Mountain Building Processes*. London: Academic Press. 19–40.
- Richter, F.M., Dauphas, N., and Teng F.Z., 2009. Non-traditional fractionation of non-traditional isotopes: evaporation, chemical diffusion and solet diffusion. *Chemical Geology*, 258: 92–103.
- Richter, F., Watson, B., Chaussidon, M., Mendybaev, R., and Ruscitto, D., 2014. Lithium isotope fractionation by diffusion in minerals, part 1: pyroxenes. *Geochimica et Cosmochimica Acta*, 126: 352–370.
- Rickwood, P.C., 1989. Boundary lines within petrologic diagrams which use oxides of major and minor elements. *Lithos*, 22(4): 247–263.
- Romer, R.L., Meixner, A., Förster, H.J., 2014. Lithium and boron in late-orogenic granites isotopic fingerprints for the source of crustal melts? *Geochimica et Cosmochimica Acta*, 131: 98–114.
- Rudnick, R.L., Tomascak, P.B., Njo, H.B., and Gardner, L.B., 2004. Extreme lithium isotopic fractionation during continental weathering revealed in sapolites from South Carolina. *Chemical Geology*, 212: 45–57.
- Su, A.N., Li, Z.Z., Tian, S.H., Hou, Z.Q., Hou, K.J., Gao, Y.G., Li, Y.H., and Yang, Z.S., 2010. Lithium isotope: analytical methods and its application to carbonatite in continental rift environment. *Mineral Deposits*, 29(5): 827–842 (in Chinese with English abstract).
- Su, A.N., Tian, S.H., Li, Z.Z., Hou, Z.Q., Hou, K.J., Hu, W.J., Gao, Y.G., Yang, D., Li, Y.H., and Yang, Z.S., 2011. High-precision measurement of lithium isotope using MC-ICP-MS. *Earth Science Frontiers (China University of Geosciences (Beijing); Peking University)*, 18(2): 304–314 (in Chinese with English abstract).
- Sun, H., Gao, Y.J., Xiao, Y.L., Gu, H.O., and Casey, J.F., 2016. Lithium isotope fractionation during incongruent melting: constraints from post-collisional leucogranite and residual enclaves from Bengbu uplift, China. *Chemical Geology*, 439: 71–82.
- Sylvester, P.J., 1989. Post-collisional alkaline granite. *Journal of Geology*, 97: 261–280.
- Sylvester, P.J., 1998. Post-collisional strongly peraluminous granites. *Lithos*, 45: 29–44.
- Tang, Y.J., Zhang, H.F. and Ying, J.F., 2007. Review of the lithium isotope system as a geochemical tracer. *International Geology Review*, 49(4): 374–388.
- Tang, Y.J., Zhang, H.F., and Ying, J.F., 2009. Discussion on Fractionation Mechanism of Lithium Isotopes. *Earth Science-Journal of China University of Geosciences*, 34(1): 43–55 (in Chinese with English abstract).
- Tang, Y.J., Zhang, H.F., and Ying, J.F., 2011. Sr-Nd-Li isotopic constraints on the origin of EM1 end-member. *Bulletin of mineralogy, Petrology and Geochemistry*, 30(1): 12–17 (in Chinese with English abstract).
- Teng, F.Z., McDonough, W.F., Rudnick, R.L., Dalpé, C., Tomascak, P.B., Chappell, B.W., and Gao, S., 2004. Lithium isotopic composition and concentration of the upper continental crust. *Geochimica et Cosmochimica Acta*, 68: 4167–4178.
- Teng, F.Z., McDonough, W.F., Rudnick, R.L., Walker, R.J., and Sirbescu, M.J.C., 2006. Lithium isotopic systematics of granites and pegmatites from the Black Hills, South Dakota. *American Mineralogist*, 91: 1488–1498.
- Teng, F.Z., Rudnick, R.L., McDonough, W.F., Gao, S., Tomascak, P.B., and Liu, Y.S., 2008. Lithium isotopic composition and concentration of the deep continental crust. *Chemical Geology*, 255: 47–59.
- Teng, F.Z., Rudnick, R.L., McDonough, W.F., and Wu, F.Y., 2009. Lithium isotopic systematics of A-type granites and their mafic enclaves: further constraints on the Li isotopic composition of the continental crust. *Chemical Geology*, 262: 370–379.
- Tian, S.H., Hou, Z.Q., Su, A.N., Hou, K.J., Hu, W.J., Li, Z.Z., Zhao, Y., Gao, Y.G., Li, Y.H., Yang, D., and Yang, Z.S., 2012. Separation and precise measurement of lithium isotopes in three reference materials using Multi Collector-Inductively Coupled Plasma Mass Spectrometry. *Acta Geologica Sinica (English Edition)*, 86(5): 1297–1305.
- Tomascak, P.B., 2004. Developments in the understanding and application of lithium isotopes in the earth and planetary sciences. *Reviews in Mineralogy and Geochemistry*, 55: 153–195.
- Tomascak, P.B., Langmuir, C.H., Le Roux, P.J., and Shire, S.B., 2008. Lithium isotopes in global mid-ocean ridge basalts. *Geochimica et Cosmochimica Acta*, 72: 1626–1637.
- Wang, H.Q., Sun, H., Liu, H.Y., and Xiao, Y.L., 2017. Lithium Isotopic Geochemistry in subduction zones: retrospects and prospects. *Acta Geologica Sinica (English Edition)*, 91(2): 688–710.
- Wang J.L., Li B.Z., and Zhou D.X., 1994. Geological characteristics and related mineralization of middle-acid complex in Heibei province. Beijing: Geological Publishing House, 213 (in Chinese).
- Xu, Z.G., Chen, Y.C., and Wang, D.H., 2008. The division of chinese metallogenic belt. Beijing: Geological Publishing House, 138 (in Chinese).
- Yang, F.L., Niu, B.G., Ren, J.S., and Li, S., 2015. Zircon U-Pb ages and geochemical characteristics of the Mesozoic intrusive bodies along the core of the Malanyu anticline and their tectonic significances. *Acta Geoscientia Sinica*, 36(4): 455–465 (in Chinese with English abstract).
- Ye, D.L., Tai, D.Q., and Ren, Y.X., 1987. Geological and petrological characteristics of M111 rare metal-bearing granite intrusion in Xinglong, Heibei. *Earth Science*, 12(3): 265–275 (in Chinese with English abstract).
- Ye, D.L., Ren, Y.X., and Tai, D.Q., 1991. The study on the characteristics of geochemistry and mineralization of the M111 rare metal contained granitic intrusion in Xinglong, Heibei. *Geoscience*, 5(1): 13–23 (in Chinese with English abstract).
- Ye, S., Zhou, B.X., and Ye D.L., 2015. Characteristics of the rare metal granite and its mineralization. *Acta Petrologica Et Mineralogica*, 34(5): 767–776 (in Chinese with English abstract).
- Zack, T., Tomascak, P.B., Rudnick, R.L., Dalpé, C., and McDonough, W.F., 2003. Extremely light Li in orogenic eclogites: the role of isotope fractionation during dehydration in subducted oceanic crust. *Earth and Planetary Science Letters*, 208: 279–290.
- Zhao, Y., Hou, K.J., Tian, S.H., Yang, D., and Su, A.N., 2015. Study on measurements of lithium isotopic compositions for common standard reference materials using multi-collector inductively coupled plasma-mass spectrometry. *Rock and Mineral Analysis*, 34(1): 28–39 (in Chinese with English abstract).
- Zhao, Y., Zhai, M.G., Chen, H., and Zhang, S.H., 2017. Paleozoic–early Jurassic tectonic evolution of North China Craton and its adjacent orogenic belts. *Geology in China*, 44 (1): 44–60 (in Chinese with English abstract).

About the first and corresponding author



HOU Jianglong, male; born in 1988 in Xingtai City, Hebei Province; postdoctor; graduated from Chinese Academy of Geological Sciences. He is now interested in the study on mineralization of rare metal deposits. Email: houjianglong1988@126.com. phone: 15110130157.